J Nanopart Res (2021) 23: 138
https://doi.org/10.1007/s11051-021-05244-y

RESEARCH PAPER

On thermal stability of nanocrystalline Ag–Cu-S powders

Jiří Sopoušek · Dáša Drenčaková · Pavel Brož · Jiří Buršík · Adéla Zemanová · Pavla Roupcová

Received: 30 December 2020 / Accepted: 23 May 2021 / Published online: 30 June 2021

Abstract The nanocrystalline semiconducting compounds based on the AgCuS system are considered as low-cost candidates of thermoelectric materials with improved thermal stability. The nanocrystalline Ag–Cu—S powders were prepared from metal nitrates and sulphur powder in tetraethylene glycol (TEG) solvent by reductive agent $NaBH_4$. The crystallite sizes of the observed phases were in the range between 60 and 80 nm. The chemical compositions of the as-received samples were analysed by the ICP-AES method and their phase compositions were evaluated by XRPD. The investigation was supplemented by DSC and in situ HTXRD thermal analysis. A more detailed in situ experiment was performed for a sample containing ternary phases. The nucleation and growth of silver micro-wires were first observed on the substrate involving ternary phases at isothermal heat treatment. The formation of silver wires and semi-conductive ternary thermoelectric phase (stromayerite τ_3) is explained by observed phase transformation. The obtained results are complemented by microscopy (LM, SEM, TEM).

Keywords Nanoparticles · Thermoelectrics · DSC · In situ XRPD · Stromayerite · Silver wires

J. Sopoušek (✉) · D. Drenčaková · P. Brož
Faculty of Science, Department of Chemistry, Masaryk University, Kotlářská 2, 611 37 Brno, Czech Republic
e-mail: sopousek@mail.muni.cz

J. Sopoušek · P. Brož
Central European Institute of Technology, CEITEC, Masaryk University, Kamenice 753/5, 625 00 Brno, Czech Republic

J. Buršík · A. Zemanová · P. Roupcová
Institute of Physics of Materials, Academy of Sciences of the Czech Republic, Žižkova 22, 616 62 Brno, Czech Republic

P. Roupcová
Brno University of Technology, Central European Institute of Technology, Purkyňova 123, 612 00 Brno, Czech Republic

Introduction

Awareness of the behaviour of minerals based on the Ag–Cu–S system has a deep history. The minerals that make up sulphur with silver and copper have been of interest since the early days of mining and metallurgy.

Scientific research in our sense began at the beginning of the twentieth century, when the pseudo-binary diagram Ag_2S–Cu_2S (Friedrich 1907) was observed by K. Friedrich. A thorough examination of the pseudo-binary diagram and extension to the ternary diagram of Ag–Cu–S was performed later by Harlov (Harlov and Sack 1995).

The ternary phases of the Ag–Cu–S system are already described by Djurle et al. in reference (Djurle et al. 1958) and in particular by Skinner (Skinner 1966; Skinner et al. 1966). The latest summary information

including a crystallographic description of phases, thermodynamic properties and several isothermal phase diagrams was given in 2006 by G. Effenberg (Materials Science International Team MSIT® 2006). The pseudo-binary diagram of Ag_2S-Cu_2S is shown in Fig. 1 and an isothermal section of the Ag–Cu–S system is shown in Fig. 2. Unfortunately, the complex assessment of the Ag–Cu–S system by the usual CALPHAD method (Saunders and Miodownik 1998) has not been carried out yet.

The renaissance of chalcogenide-based materials has occurred in connection with the search for thermoelectric materials capable of converting thermal energy into electrical energy (He and Tritt 2017; Liang et al. 2017; Zheng et al. 2018). New promising bulk thermoelectrics: intermetallics, pnictides and chalcogenides, are described in Gonçalves and Godart (2014). The object of the thermoelectric search is mainly metal chalcogenides for their cheapness and nontoxicity (Gonçalves and Godart 2014; Lokhande et al. 2016). Promising thermoelectrics are also Cu-chalcogenide-based materials (Qiu et al. 2016).

The empirical parameter "figure of merit ZT" was introduced for a general assessment of thermoelectric properties of studied materials. The value of ZT had been observed for copper chalcogenide thermoelectric materials in the range of 0–2.7 (Wei et al. 2019). The high ZT does not mean that the material is a practically usable thermoelectric neither if the colossal Seebeck effect measured for Cu_2Se (Byeon et al. 2019).

The ternary phases of the Ag–Cu–S system are semiconductors. A more detailed study of the structure and lattice dynamics of copper- and silver-based superionic conducting chalcogenides and especially the properties of the jalpaite ternary phase were investigated by Trots and co-workers (Trots et al. 2008). The ternary phase of τ_3 stromayerite has been shown to be a thermoelectric material although not having a very high ZT factor.

To study pure ternary phases, syntheses of complex sulphides of AgCuS and Ag_3CuS_2 from the elements under hydrothermal conditions were proposed by Tokuhara (Tokuhara et al. 2009). Attention is also paid to the synthesis and research of the properties of bulk materials based on binary systems Ag–S (Živković et al. 2013) and Cu–S (He et al. 2014; Jiang et al. 2014).

The recent investigations move from bulk material research to nanomaterials (Alam and Ramakrishna 2013) and nanocomposites (Liu et al. 2012). It is also a new impulse to improve thermoelectric materials as

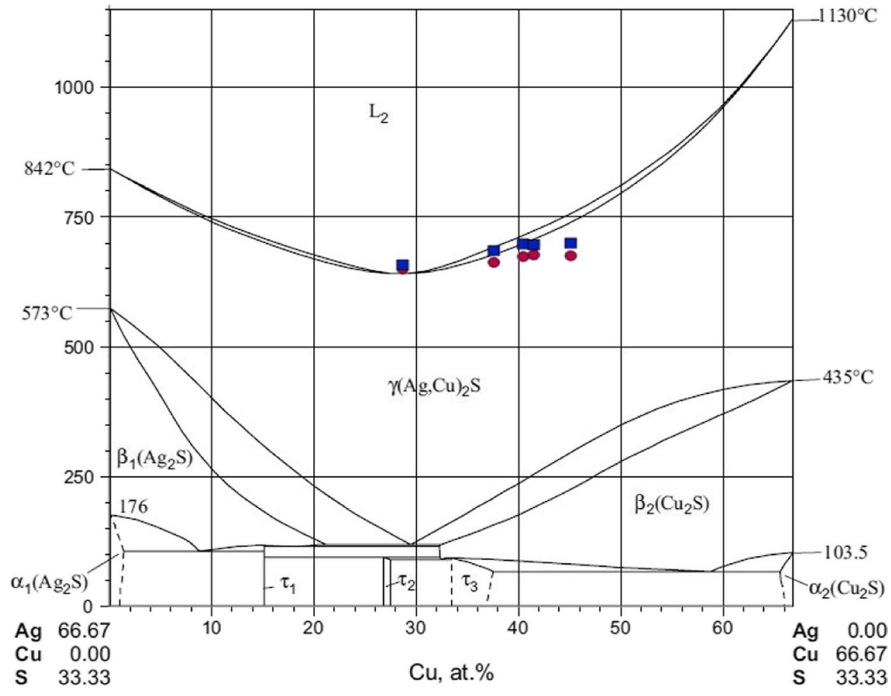

Fig. 1 The Cu_2S–Ag_2S pseudo-binary phase diagram (Materials Science International Team MSIT® 2006) complemented by the experimental results of DSC on nanocrystalline samples referred to in Table 2

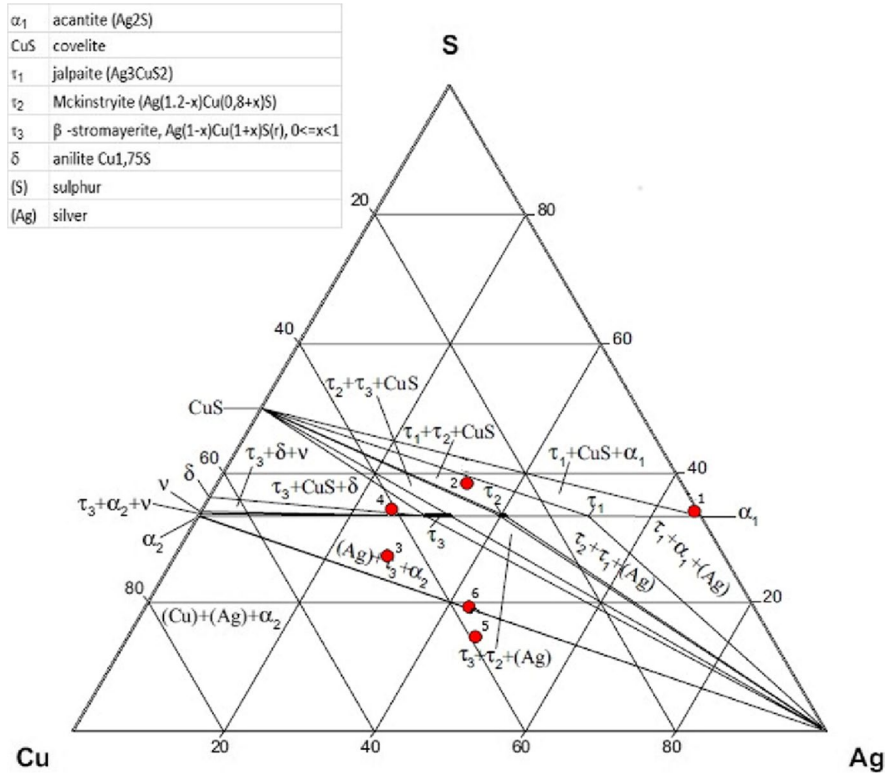

Fig. 2 The equilibrium Ag–Cu–S phase diagram (Materials Science International Team MSIT® 2006) at 25 °C complemented by overall compositions of synthetized nanocrystalline samples referred to in Table 1

can be seen in the published report (Kanatzidis 2010). It appears that nanostructuralization significantly influences the value of ZT [2010], but according to most researches, it has been rather decreased values so far.

The latest investigation of the Ag–Cu-S system again focuses on monitoring the thermoelectric properties of the τ_3 phase (stromayerite) in the bulk form (Dutta et al. 2018). However, research is also partly focused on the study of nanocrystalline powders (Guin et al. 2016). One of the variants under investigation is the preparation of nanocrystalline thermoelectrics modified by graphene (Al Alwani Ammar et al. 2019). Some conductive polymers have been proposed for the preparation of these nanotermoelectric composites (Bharti et al. 2018). The pioneering work was presented, for example, by the study of properties of CuS nanocomposite (Tang et al. 2018), but more detailed experimental studies of other nanocrystalline thermoelectric composites are still rare.

Experimental section

Materials

The following chemicals were all used as obtained: tetraethylene glycol ($C_8H_{18}O_5$, CAS 112–60-7, 99% chemical grade, AlfaAesar), sulphur (powder, CAS 7704–34-9, chemical grade: purists p. a., Lachner), polyvinylpyrrolidone (PVP, CAS 9003–39-8, chemical grade: for synthesis, Merck), sodium borohydride ($NaBH_4$, powder, 97% chemical grade for synthesis, CAS 16940–66-2), silver nitrate ($AgNO_3$, CAS 7761–88-8, chemical grade: purists p. a., Lachner), copper(II) nitrate trihydrate ($CuNO_3 \cdot 3H_2O$, CAS 10031–43-3, chemical grade: purists p. a., Penta), regenerated graphene oxide (rGO, prepared in the laboratory of Department of Chemistry according to [lit] Dr. Z. Moravec), water (deionized, < 1 µS/cm), liquid nitrogen (> 4.5 N, SIAD

Rajhrad) and ethanol (C_6H_5OH, denatured with about 1% methyl ethyl ketone).

Nanoparticle synthesis

The method reported by Guin (Guin et al. 2016) was adapted. Shortly, the samples of the AgCuS nanoparticles (AgCuS NPs) were prepared by wet synthesis from silver and copper nitrate precursors in tetraethylene glycol by use of $NaBH_4$ at laboratory temperature. The synthesized product was separated using a high-speed centrifuge. The product was purified by repeated dissolving in ethanol and by subsequent centrifuging. Some samples were prepared with the addition of PVP and rGO to the reaction mixture to stabilize and separate the individual nanoparticles of AgCuS. The samples in the form of black coloured AgCuS ethanol suspensions were obtained after purification. The drying under vacuum at laboratory temperature was used to obtain dry powder samples.

Instrumentations

Dynamic light scattering (DLS) The sonicated solutions of the prepared AgCuS samples (at 25 °C) were characterized by the DLS method on a Zetasizer Nano ZS ZEN 3500 instrument (Malvern UK) working at the scattering angle of 173°. The method measures a hydrodynamic size of NPs, which is given by both the metal core and the stabilizing organic layer of the core.

Overall chemical analysis The chemical composition of the AgCuS samples was obtained by elemental analysis. The AgCuS powder was weighed and dissolved in nitric acid at elevated temperatures. The Ag, Cu and S content was analysed by inductively coupled plasma atomic emission spectroscopy (ICP-OES) calibrated on pure metals and sulphur. The difference between the mass of the dry sample and the weight of the Ag, Cu and S elements was presumed to be the mass of organic matter.

Transmission electron microscopy (TEM and HRTEM) The metal cores of the AgCuS samples were investigated by electron microscopy because this technique is sensitive to heavier elements and less sensitive to light elements that form an organic stabilizing layer of the particles. To prepare samples, a powder was placed on a holey carbon film-coated Cu grid. The size and shape of AgCuS particle cores were investigated using a Philips CM12 STEM microscope with a thermoemission source operated at 120 kV and a JEOL JEM 2100F high-resolution TEM (HRTEM) with an FEG source operated at 200 kV (point resolution of 2.3 Å). Both transmission electron microscopes were equipped with energy-dispersive X-ray (EDX) detectors.

X-ray powder diffraction (XRPD) Measurements were carried out on a GNR Europe XRD 600 diffractometer equipped with a Co lamp, $\lambda K\alpha_{1,2} = 1.7903$ Å, 40 kV, 15 mA, with theta/2theta configuration. Samples were measured in a step scan of 0.2° for 10 s in reflection mode on plastic or aluminium sample holders. A 1D detector DECTRIS Mythen2R was used. If noted in the article, the accuracy of phase fraction is about 5 mol% and the complement to 100% are phase impurities. The XRPD method gives a size of crystallite domains (abbreviation "cryst." used).

The multipoint BET method The Quantachrome Autosorb IQ 3 helium porosimeter and at least five data points method with relative pressures between 0.05 and 0.23 was used for evaluation of the specific surface area of the samples.

High-temperature X-ray powder diffraction (HTXRD) Empyrean PANalytical (Netherlands) diffractometer with $CoK\alpha_{1,2}$ radiation and HTK 1200 Anton Paar (Austria) was used for HTXRD. The diffractograms were collected in a helium (5 N) floating atmosphere at each temperature during collecting data. The average heating rate including sample heating and hold at temperature during measurement was 5 K/min. The phase composition, lattice constants of phases and crystallinity were determined by the Rietveld method used HighScore + 4.0 equipped by ICDD database which included structural models.

Mass spectroscopy with direct input probe (DIP MS) Measurements were performed on mass spectrometer TSQ Quantum XLS with the temperature program: stabilization 30 °C for 30 s, heating 50 °C/min 30–450 °C, ionization energy 70 or 22 eV, and detector temperature was set to 200 °C.

Simultaneous thermal analysis (DSC/TGA) Three instruments were used. The thermal properties (DSC) of AgCuS samples were examined by rate 10 K min^{-1} on a Netzsch STA 409 CD/3/403/5/G apparatus under flowing (70 cm^3 min^{-1}) pure (6 N) argon from room temperature to approx. 800 °C. The oxygen-free atmosphere was maintained by a metallic zirconium trap located in the hot zone of the calorimeter. The TGA/DSC analysis was done by Netzsh STA 449 Jupiter under flowing (70 cm^3 min^{-1}) pure (4.5 N) nitrogen from room temperature to approx. 800 °C. The thermal properties (DSC) of AgCuS samples were examined on a Netzsch Pegasus 404C apparatus under flowing (50 cm^3 min^{-1}) pure (5 N) argon from room temperature to 800 °C. The samples (approx. 50–80 mg) were always measured in Y_2O_3-coated alumina crucibles covered with a lid.

Scanning electron microscopy (SEM) Morphology and overall composition of the samples were observed by scanning electron microscopy (SEM) using a TESCAN LYRA 3XMU FEG/SEM microscope with an X-Max 80 EDX Oxford Instruments detector. Field-emission scanning electron microscope (FESEM) Thermo Fisher Verios 460L working in energy range (0.7 nm @ 1 keV, 0.6 nm @ 2–30 keV) equipped with EDS analyser EDAX SDD Octane Super with energy resolution (129 eV @ MnKα).

Results and discussion

The samples in the form of the AgCuS ethanol black suspensions were investigated by the DLS method. The measurements revealed big particles and great fluctuations in hydrodynamic particle size that indicates nanoparticle aggregation. As a consequence, the synthesis was modified by the addition of the stabilizing agents: polyvinylpyrrolidone (PVP) and regenerated graphene oxide (rGO). The additions (2–3wt% of the sample weight) of rGO to suspension decreases the hydrodynamic size of particles; however, clusters of the AgCuS nanoparticles still remain in colloid solution (see Fig. 3).

Size, shape and composition of AgCuS samples were investigated in detail by electron microscopy on dried drops of sample suspensions. The samples were black powders, which all reveal the microstructures nearly the same as given in Fig. 4. At higher magnification, powders had a coral-like structure consisting of aggregated AgCuS nanoparticle units. The nanoparticle units are joined by interconnection necks (see detail in Fig. 4). The size of the nanoparticle unit was in reasonable agreement with the crystallite size obtained by the powder X-ray diffraction method (see Table 1). The same morphology of samples was presented by Guin et al. for nanocrystalline AgCuS (Guin et al. 2016). The authors have investigated the nanocrystalline phase, which was entitled AgCuS in your article (i.e., stromayerite phase τ_3 in Fig. 2).

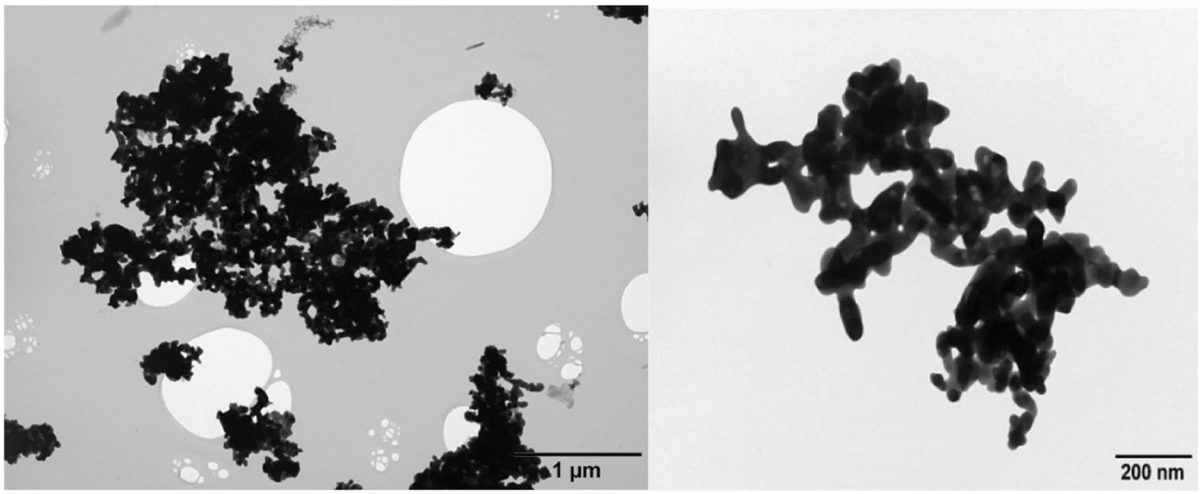

Fig. 3 Clusters of aggregated AgCuS nanoparticles. Microstructure of nanocrystalline AgCuS powder (sample 1 with rGO). Overview in left and detail in right (TEM)

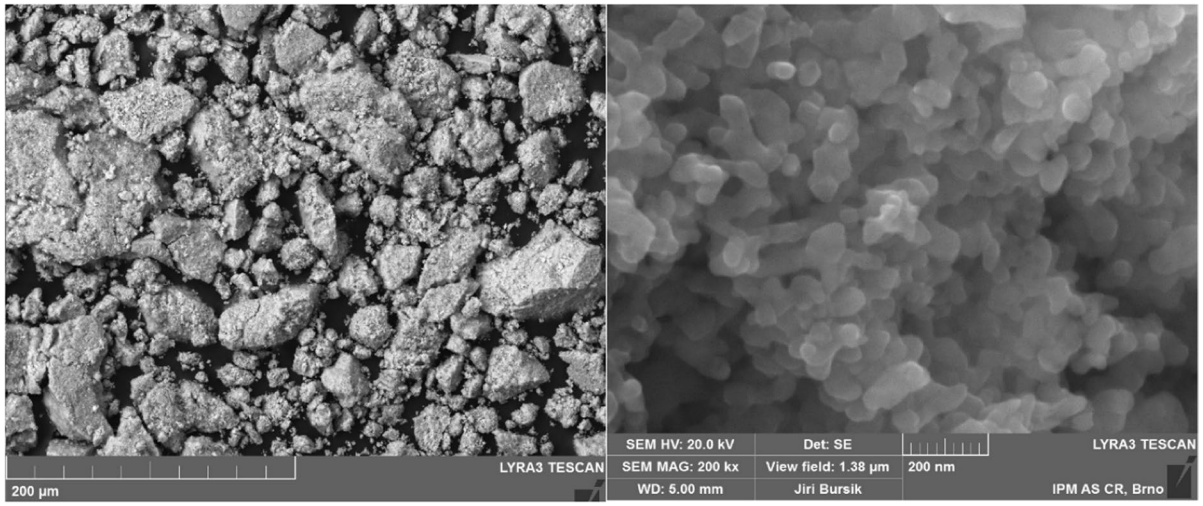

Fig. 4 Aggregated microstructure of nanocrystalline AgCuS powder (sample 4). Overview in left and detail in right (SEM)

The overall compositions of dry AgCuS samples have been measured by the ICP-AES method. The results of the analyses are given in Table 1. The chemical composition of the AgCuS powders was tested also by an EDX detector inside an electron microscope. The EDX compositions of the samples were in agreement with element analysis in Table 1 but with higher uncertainty.

The phase compositions of the dry AgCuS samples were identified by the X-ray diffraction powder method (XRPD). An example of diffraction patterns is given in Fig. 5. These measurements enabled us to identify phases in the experimental samples and to obtain the average crystallite size of the samples applying the Scherer equation (Patterson 1939) to the peaks in the XRPD experimental pattern. Moreover, the specific surface areas of samples 4 and 8 were analysed by means of BET porosimeter (see values in Table 1).

The coexisting phases identified by the XRPD method in the as-prepared AgCuS powder samples are in Table 1. The coexisting phases in bulk samples of the same chemical composition as experimental samples are given for comparison. The coexisting

Table 1 Chemical (ICP-AES) and phase compositions (XRPD) of AgCuS samples. The names of phases in bold means major phase and brackets means minor phase

Sample no	Composition/at% (stabilization)	Composition/at%			Average crystallite size according to Scherer eq./nm (surface area/$m^2\ g^{-1}$)	Coexisting phases	
		Ag	Cu	S		Experiment	Bulk equilibrium (Materials Science International Team MSIT® 2006)
1	66Ag00Cu34S (rGO)	65.6	0.4	34	106.3^{H} (11.25)	**α_1**	**α_1**
2	33Ag28Cu38S	33.3	28.4	38.4	85.62	**τ_1** + τ_2 + CuS	**τ_1** + **τ_2** + CuS
3	28Ag45Cu27S	28.2	44.6	27.2	70.85	**τ_1** + **τ_2**	**Ag** + **τ_3** + **Cu_2S**
4	25Ag40Cu34S	25.0	40	34	68.04	τ_1 + **τ_2**	**τ_3** + CuS + δ
5	29Ag41Cu30S (PVP)	28.6	41	30.4	(7.04)	**Cu_2S** + CuS + (CuO) + (Ag)	**Ag** + **Cu_2S** + (Cu)
6	25Ag37Cu38S (rGO)	25.0	37.2	37.8	-	τ_2 + CuS	**Ag** + **Cu_2S** + (τ_3)

Legend: $\alpha_{1...}$ acanthite (Ag_2S), CuS… covelite, Cu_2S… $(Ag,Cu)_2S$, $\tau_{1...}$ jalpaite (Ag_3CuS_2), $\tau_{2...}$ mckinstryite ($Ag_{(1.2-x)}Cu_{(0,8+x)}S$), $\tau_{3...}$β—stromayerite, $Ag_{(1-x)}Cu_{(1+x)}S$ ($0 \le x < 1$), δ… anilite $Cu_{1,75}S$, (S)… sulphur, (Ag)…silver, (Cu)…copper, rGO…reduced graphene oxide, PVP…polyvinylpyrrolidone. ^{H} …after heating to 300 °C and cooling during DSC measurement

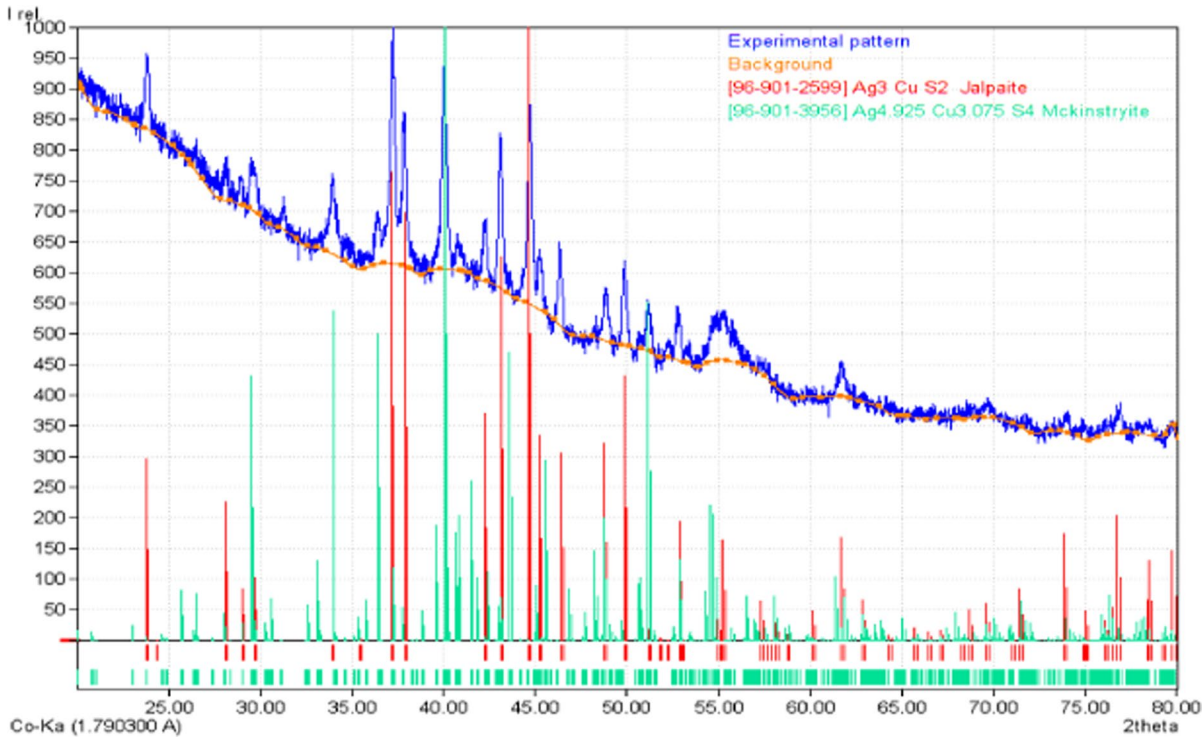

Fig. 5 The powder X-ray powder diffraction pattern of the AgCuS sample (6)

phases in bulk material were obtained from Fig. 2, which shows the phase ternary diagram of the Ag–Cu–S system at 25 °C (Materials Science International Team MSIT® 2006).

The agreement in phase composition exists for sample 1 or 2. In the other cases, the phase compositions differ and show that used nanoparticle synthesis incline to form more simple phases (binary sulphides). The ternary semi-conductive phase $\boldsymbol{\tau_3}$ (stromayerite, AgCuS) was not prepared by our way of synthesis. Instead of $\boldsymbol{\tau_3}$, the ternary phases $\boldsymbol{\tau_1}$ (jalpaite Ag_3CuS_2) and $\boldsymbol{\tau_2}$ (mckinstryite, $Ag_{3.925}Cu_{3.075}S_2$) were found in yield.

In general, the inorganic nanoparticles are usually covered by a big portion of organic matter that has an origin in chemical synthesis and it is difficult to remove organic matter from the samples without great particle loss. It was also observed in our experiment. The mass of organic matter in the nanocrystalline AgCuS powders was evaluated from the difference between sample weight and the mass sum of elements of Ag, Cu and S obtained by ICP-AES analysis. The organic matter content in the nanocrystalline AgCuS powders was in the range of 22 (sample 4) minima to 58 (sample 2) maxima wt%. Samples 1 and 6 with rGO and PVP were overweight by organic matter. The matter difference was a function of the purification procedure.

The stability of the nanocrystalline AgCuS powders without rGO was investigated by DIP MS. The results are given in Fig. 6. The investigated sample 4 evolves the signals of organic matter origin (mainly tetraethylene glycol fragments and PVP). The increased instability occurred at a higher temperature above approximately 300 °C. Above other the M/z Eq. 63.68 has occurred. It indicates SO_2 evolution in the instability region. The SO_2 evolution has occurred for all experimental samples at temperatures about 300 °C.

The nanocrystalline AgCuS powders with rGO were investigated by the DSC method using three different instrumentations. The DSC/TGA investigation was dome by Netzsch STA 449 Jupiter in 5 N nitrogen carrier gas. The investigated sample 1 (composition is close to Ag_2S compound) reveals a low 2.6% weight loss with a maximum rate of change at

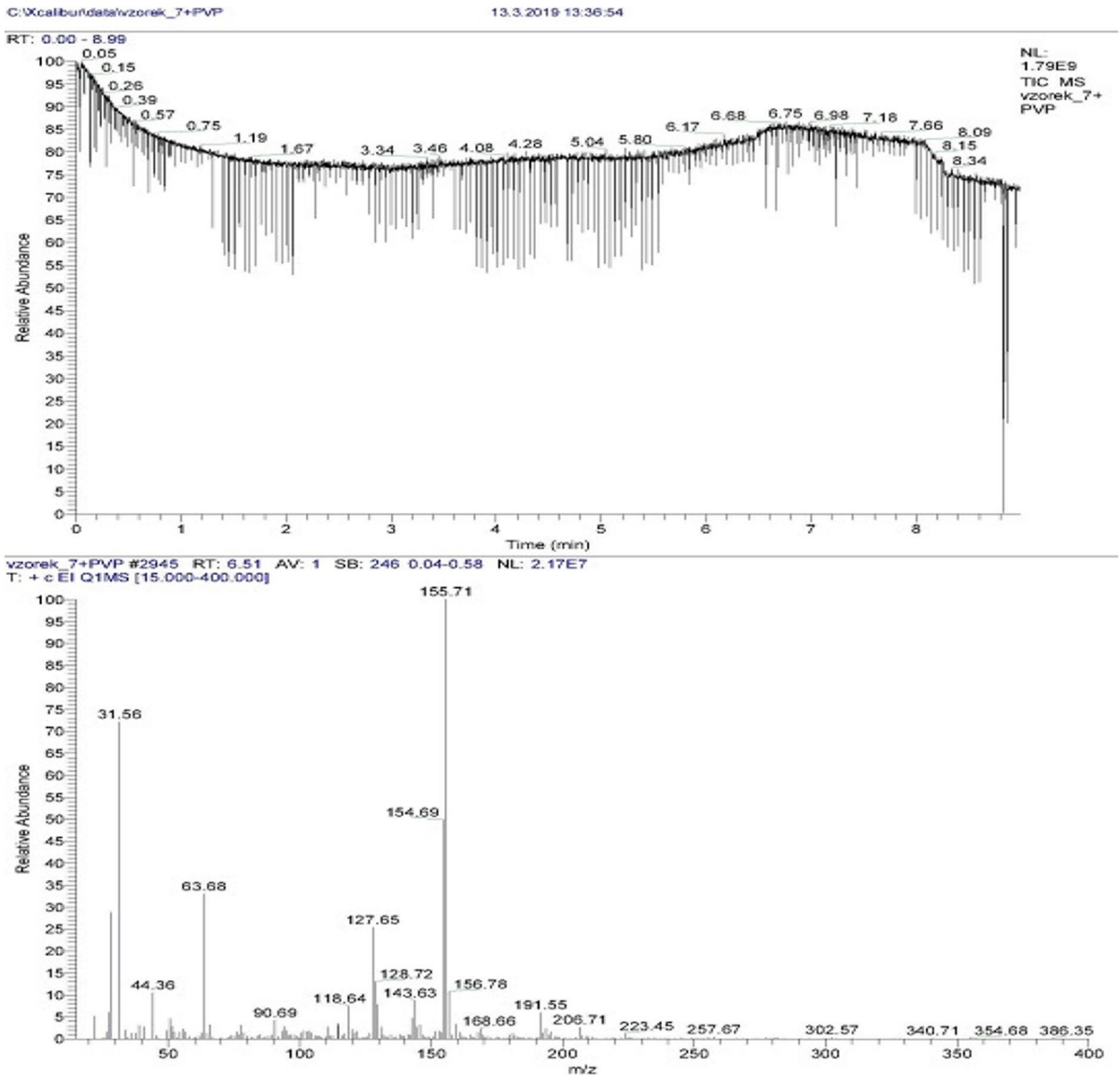

Fig. 6 DIP MS measurement of the nanocrystalline AgCuS powder (sample 4). Sample heated from laboratory temperature with rate 50 °C/min. Upper: mass outflow from the sample. Below: MS spectrum at 6.51 min (i.e., at approx. 305 °C)

196 °C. The weight was then stable up to 700 °C. The DSC signal reveals an endothermic signal (onset at 168 °C) followed by an exothermic effect with maxima of 207 °C.

The origin of the endothermic effect seems to be in agreement with the phase transformation of the Ag_2S compound α_1-Ag_2S (acanthite) $\rightarrow$ β-Ag_2S (argentite), which is referred in Sharma and Chang (1986); Sadovnikov et al. 2018) at 178 °C. The 10 °C difference can be explained as phase transformation depression due to nanocrystallites or experimental uncertainty. The exothermic effect at 207 °C seems to be the combustion of organic matter with traces of oxygen in nitrogen carrier gas because it was not observed if an extra pure argon gas by Netzsch STA 409 (see details in the Instrumentations section) was used. The particle layer from rGO (or its carbonization product) seems to be stable in oxygen-free gas to high temperatures.

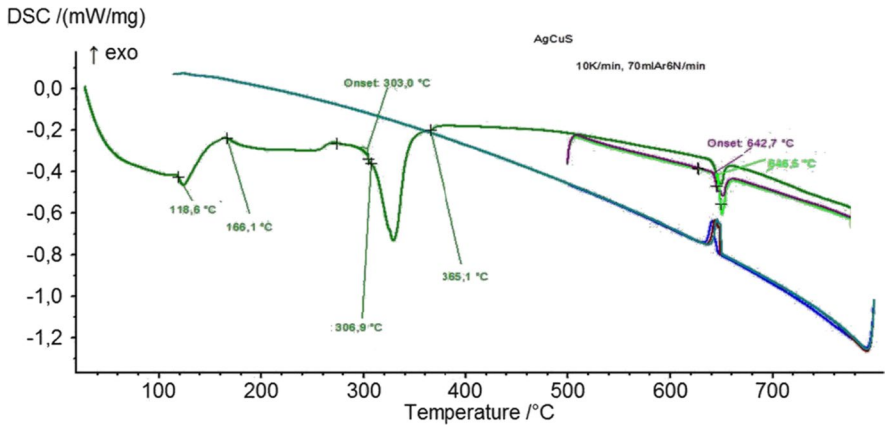

Fig. 7 DSC analysis of nanocrystalline sample 2 by Netzsch Pegasus 404C (10 K/min, 5 N Ar). Low-temperature range A (25–280 °C). Central temperature range B (approx. 280–500 °C). Temperature cycling at high-temperature range C (500–800 °C)

The heating effects, liquidus and solidus temperature, were evaluated also by the Netzsch Pegasus 404C apparatus. The DSC signal of the samples was similar (see example in Fig. 7) and can be divided into three parts A, B and C.

The low-temperature range A exists up to approx. 280 °C. At this temperature range, we suppose evaporation of solvent traces and low-temperature phase transformations of ternary phases (see Fig. 1). The onsets of decompositions are given in Table 2.

The most intensive heat endothermic effect can be found in central temperature range B (approx. 280–450 °C). This intensive heat effect does not exist if argon carrier gas was free of oxygen traces (use Netzsch STA 409, see details in the Instrumentations section). The endothermic peak occurs in the presence of at least a trace amount of oxygen at temperatures where the formation of sulphur dioxide has been detected (see MS spectrum in Fig. 6).

At high-temperature range C (450–800 °C), the samples reveal melt and crystallization. The solidus and liquidus temperatures were evaluated using special method published in Boettinger et al. (2006) and the values are plotted in Cu_2S-Ag_2S pseudo-binary phase diagram in Fig. 1.

The DSC measurement indicates more events of phase transformations (τ_1, τ_2) (Materials Science International Team MSIT® 2006) at low-temperature region 25–125 °C, but due to the sensitivity limit of used instrumentation, the signals cannot be evaluated (see Fig. 7). In the central temperature range, an unclear endothermic effect was observed. This endothermic effect was not present if extra pure argon was used by Netzsch STA 409 instrumentation. The endothermic effect may be associated with some decomposition reaction when the sample is heated. The melting of the samples at high-temperature range C was occurred. The experimental results are summarized in Table 2.

Table 2 Temperatures (in Celsius) obtained via DSC measurement of nanocrystalline AgCuS powders (Netzsch Pegasus 404C apparatus using 5 N argon, impurities: N_2 and O_2)

Sample no	Decomposition of ternary phases	Maxima for organic matter combustion	Onset of big endothermic signal	Onset of unidentified phase change	Solidus	Liquidus
1 [Zr]	-	-	-	-	653	695
2 [5 N]	118	166	303	365	644.6	652.45
3 [5 N]	101	193	313	417	670	693.95
4 [5 N]	-	-	-	379	668.2	692.9
5 [5 N]	112	187	337	-	671.6	690.95
6 [5 N]	100	186	301	411	656.95	679.7

[Zr] …measured by Netzsch STA 409 using argon purified by Zr

Spontaneous Ag micro-wire growth

Sample 2 was examined in more detail by in situ HTXRD when it was gradually heated to 400 °C and cooled to room temperature under pure helium gas. The XRD measurements were performed at 25 °C and isothermal delays at 100, 150, 200, 250, 275, 300, 310, 320, 350 and 400 °C. The time of each isothermal delay was 20 min. Among other things, the fractions of the identified phases and their crystallinity were evaluated from the measurements. Experiments were conducted with the sample 2 as synthesized with phase composition: (64% τ_1 (crystallinity 65 nm) + 22% τ_2 (cryst. 53 nm) + 14%CuS (cryst. 10 nm)).

During the heating of sample 2, phase τ_2 disappeared at a temperature somewhere between 25–100 °C. Phase τ_1 disappeared at a temperature between 100 and 150 °C. The CuS phase disappeared at a temperature between 300 and 310 °C. At a temperature between 150 and 200 °C, a new phase appeared in the XRPD sheet. This phase should be mixed sulphide phase γ-$(Ag,Cu)_2S$ with antifluorite crystal structure (Skinner 1966; Du et al. 2017) (see Fig. 1), but our data do not confirm the existence of that phase. Other possibilities are as well of presence impurities evaporated from the chamber or chemical reaction this vapours with the sample. The XRD pattern was not found in the available crystallographic databases PDF2 (2017), COD (2019) and PDF4; this may be because γ-$(Ag,Cu)_2S$ is not quenchable (Newman et al. 1982). The significant amorphization of the sample is visible at 200 and 310 °C by loss of crystalline fraction.

When cooling sample 2 from a temperature of 400 °C, the γ-$(Ag,Cu)_2S$ phase disappeared somewhere between 200 and 100 °C. Phase τ_2 reoccurred between 100 and 25 °C. The new low-temperature semi-conductive phase: τ_3 stromayerite appeared between 100 and 25 °C. At the same time, the formation of elemental Ag in the form of micro-wires was observed first at these conditions. A subsequent experiment was devoted to this phase transformation effect.

The weight of sample 2 as synthesized was heated to 600 °C, annealed for 200 min and cooled to room temperature. The result was the growth of silver micro-wires on sample 2 to a greater extent, as evidenced by the photo in Figs. 8 and 9. The diameter of these wires was about 2 µm and the bundles of these wires reached a size of up to 0.1 mm. The length of silver wires reaches about 7 mm. The individual wires seem to be single crystals (pure Ag) in contrary to finding in natural silver wires (Boellinghaus et al. 2018), synthetic silver wires above acanthite (Anderson et al. 2019) or at silver corrosion (whisker formation) (Chudnovsky et al. 2002).

Silver nucleation and its growth in wire form is obviously related to the reduction of sulphur content in the sample at higher temperatures (compare the detection of SO_2 in Fig. 6). In Fig. 9, we see that the wires grow on nucleation centres, which are

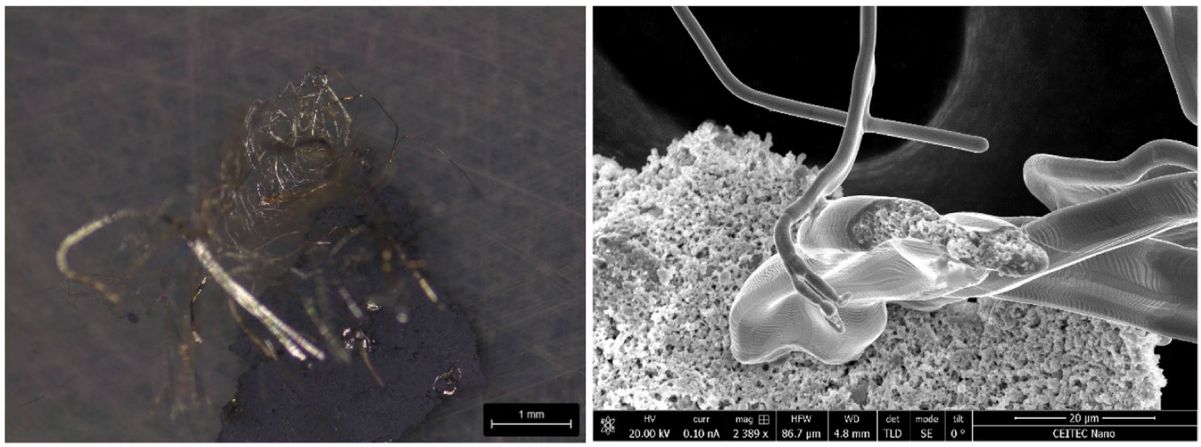

Fig. 8 Nanocrystalline sample 2 after isothermal heating at 600 °C/200 min. The Ag micro-wires growing on (stromayerite + τ_2) substrate. Left: light microscopy. Right: SEM detail of joining between Ag wires and substrate

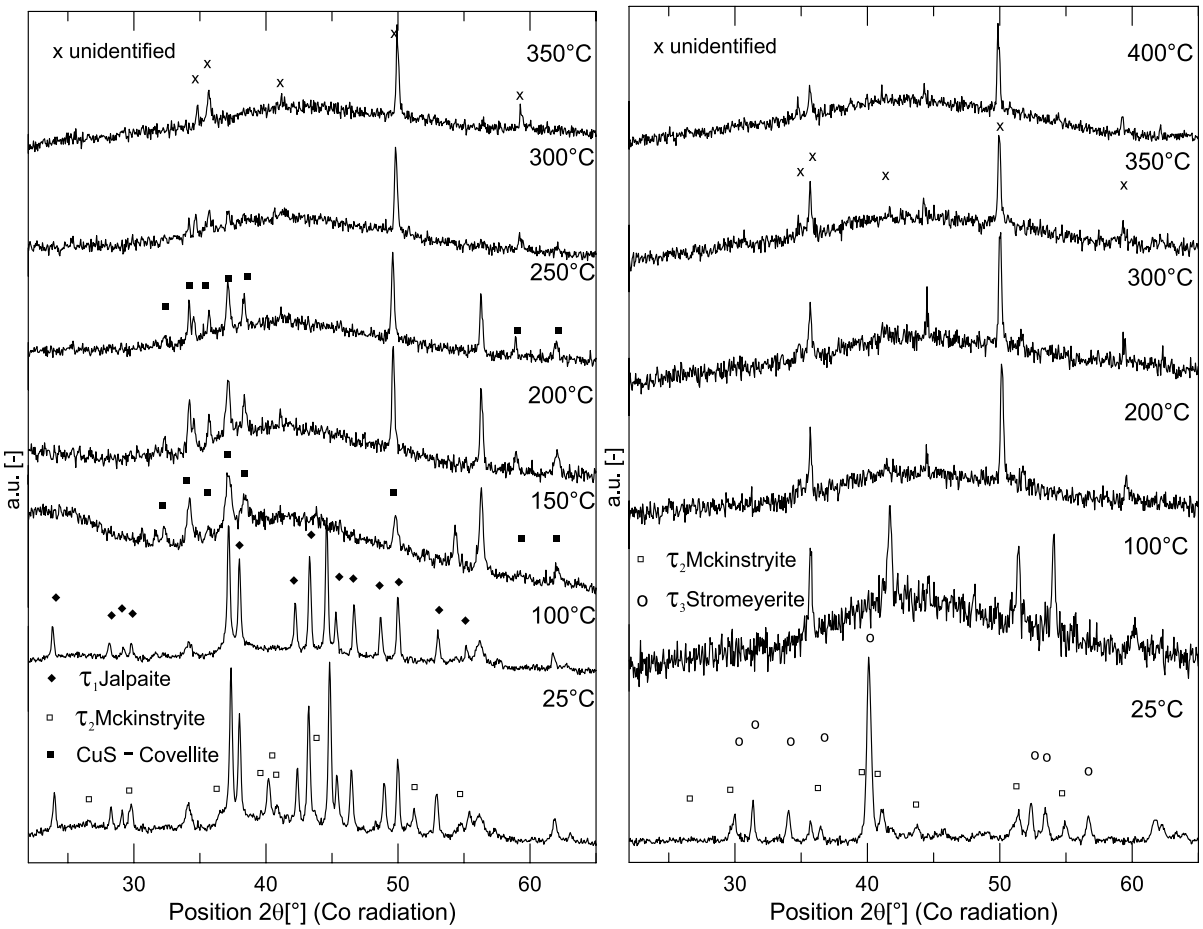

Fig. 9 X-ray powder diffraction sheet of sample 2 before heating ($\tau_1+\tau_2+$CuS), at higher temperatures (unidentified phase), and after cooling to 25 °C ($\tau_2+\tau_3$)

located on the surface of sample 2. The EDX analysis confirmed that the composition of the wires is pure silver and the rest of sample 2 is composed of subsequent phases: stromayerite (64% of ternary phase τ_2, cryst. 40 nm) and mckinstrite (τ_2, 34%, cryst. 42 nm). The HT XRD measurement during this experiment is in Fig. 10. The XRD mapping of chemical elements of the junction between wires and rest of the sample 2 is shown in Fig. 10. The growth of wires is influenced also by the temperature gradient inside the device, because the sample is heated by contact with the silicon support.

The result of the experiment is a composite material (see Fig. 8) containing stromayerite (considered as a thermoelectric) and mckinstryite joined with pure silver wires that can serve as electrical contacts.

Conclusions

The synthesized AgCuS nanoparticles were prepared and characterized. The test of using PVP and rGO for better stabilization of the samples in colloids. The differences between as-synthesized and equilibrium phase compositions were found. It turned out that the experimental phase composition of nanostructured samples does not contain ternary phases exactly according to the equilibrium diagram for a compact material of the same chemical composition (see Table 1).

The temperature stability of AgCuS samples was investigated by DSC and DIP MS. Both endothermic and exothermic effects were measured within the DSC experiment (see Table 2). The endothermic effects correspond to the decomposition of the

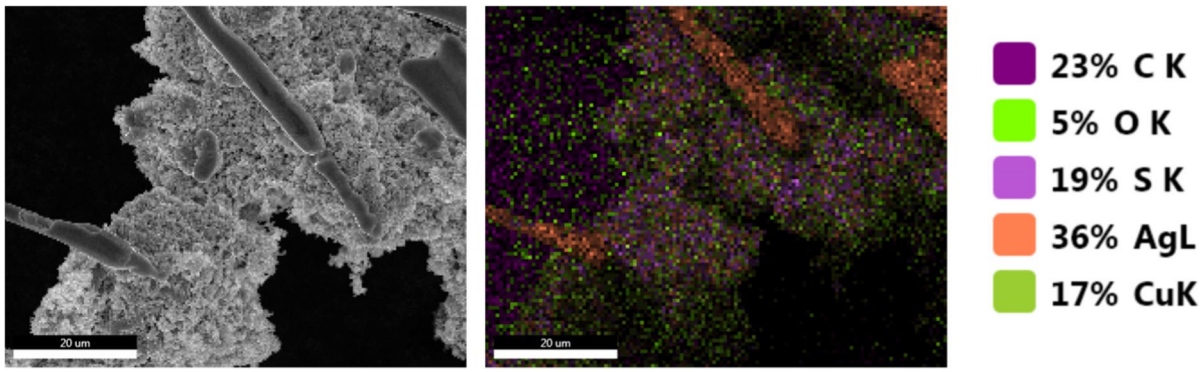

Fig. 10 Sample 2: detail of Ag nanowire joining with the substrate after HT XRPD analysis (annealed at 600 °C/200 min). SEM (left) photo and EDX (right) analysis by EDAX

ternary phases and the melting of the samples (see Fig. 1). In the mean temperature range for all samples, a strong endothermic signal was observed (around 300–350 °C), which may be related to a change in chemical composition due to the release of SO_2. Exothermic signals correspond to organic matter combustion.

Nucleation and growth of pure silver wires were observed in sample 2 with a composition of 33% Ag28% CuS (see Fig. 10). In a more detailed XRPD experiment, it was possible to identify not only the initial low-temperature phases but also the phase occurring at a medium temperature range of 200–400 °C. This phase should be the γ-$(Ag,Cu)_2S$ phase. However, this has not been confirmed. On heating, on the other hand, the amorphous phase and a small amount of a new unidentifiable phase were formed (see Fig. 10). After cooling to room temperature, not only wire silver was observed, but in the rest of the sample the mckinstryite and stromayerite phases. The second of these phases is considered a potential thermoelectric. In addition, after cooling of sample 2, the nano-structuring formed at synthesis was still preserved. The heating experiment was therefore repeated under conditions of isothermal annealing at 600 °C/200 min when it was possible to grow Ag wires up to 7 mm in size.

The original experiments monitoring the temperature transformations of the AgCuS system are, according to the research performed, of an older date. The use of methods available today shows that some experimental information needs to be refined.

Acknowledgements We acknowledge CzechNanoLab Research Infrastructure supported by MEYS CR (LM2018110) for FESEM imaging.

Author contributions Not applicable.

Funding Financial support of the Czech Science Foundation for the project "Thermal and phase stability of advanced thermoelectric materials" (GA 17-12844S) is gratefully acknowledged.

Data availability All data can be published publicly.

Code availability Not applicable.

Compliance with ethical standards

Conflict of interest The authors declare that they have no conflict of interest.

References

Alam H, Ramakrishna S (2013) A review on the enhancement of figure of merit from bulk to nano-thermoelectric materials. Nano Energy 2:190–212. https://doi.org/10.1016/j.nanoen.2012.10.005

Al Alwani Ammar J, Shipra P, Shiv P, Kletsov Alexey A, Venig S, Glukhovskoy Evgeny G (2019) Effect of the graphene sheets on the physical properties of copper sulfide nanoparticles. Int J Nanoparticles Nanotechnol 5. https://doi.org/10.35840/2631-5084/5529

Anderson CJ, Mathur R, Rakovan J, Tremsin AS (2019) Natural solid-state ion conduction induces metal isotope fractionation. Geology 47:617–621. https://doi.org/10.1130/G45999.1

Bharti M, Singh A, Samanta S, Aswal DK (2018) Conductive polymers for thermoelectric power generation. Prog Mater Sci 93:270–310. https://doi.org/10.1016/j.pmatsci.2017.09.004

Boettinger JW, Kattner UR, Moon K-W (2006) DTA and heat-flux DSC meassurements of alloy melting and freezing, Perepezko, J.H., NIST Recommended Practice Guide

Boellinghaus Th, Lüders V, Nolze G (2018) Microstructural insights into natural silver wires. Sci Rep 8:9053. https://doi.org/10.1038/s41598-018-27159-w

Byeon D, Sobota R, Delime-Codrin K, Choi S, Hirata K, Adachi M, Kiyama M, Matsuura T, Yamamoto Y, Matsunami M, Takeuchi T (2019) Discovery of colossal Seebeck effect in metallic Cu2Se. Nat Commun 10:72. https://doi.org/10.1038/s41467-018-07877-5

Chudnovsky BH, Swindler DL, Thompson JR (2002) A touch of gray [power contacts, silver corrosion, whiskers growth]. IEEE Ind Appl Mag 8:45–52. https://doi.org/10.1109/MIA.2002.1028390

Djurle S, Sørensen P, Stenhagen E, Hartiala K, Veige S, Diczfalusy E (1958) An X-ray study on the system Ag-Cu-S. Acta Chem Scand 12:1427–1436. https://doi.org/10.3891/acta.chem.scand.12-1427

Dutta M, Sanyal D, Biswas K (2018) Tuning of p–n–p-type conduction in AgCuS through cation vacancy: thermopower and positron annihilation spectroscopy investigations. Inorg Chem 57:7481–7489. https://doi.org/10.1021/acs.inorgchem.8b01246

Du B, Zhang R, Chen K, Mahajan A, Reece MJ (2017) The impact of lone-pair electrons on the lattice thermal conductivity of the thermoelectric compound $CuSbS_2$. J Mater Chem a 5:3249–3259. https://doi.org/10.1039/C6TA10420G

Friedrich K (1907) The fusion diagram of binary systems sulfur - silver - copper and lead -copper - sulfur. Metallurgie 4:671–673

Gonçalves AP, Godart C (2014) New promising bulk thermoelectrics: intermetallics, pnictides and chalcogenides. Eur Phys J B 87:1. https://doi.org/10.1140/epjb/e2014-40989-3

Guin SN, Sanyal D, Biswas K (2016) The effect of order–disorder phase transitions and band gap evolution on the thermoelectric properties of AgCuS nanocrystals. Chem Sci 7:534–543. https://doi.org/10.1039/C5SC02966J

Harlov DE, Sack RO (1995) Thermochemistry of Ag2S-Cu2S sulfide solutions: constraints derived from coexisting Sb2S3- and As2S3-bearing sulfosalts. Geochim Cosmochim Acta 59:4351–4365. https://doi.org/10.1016/0016-7037(95)00308-M

He J, Tritt TM (2017) Advances in thermoelectric materials research: looking back and moving forward. Science 357:eaak9997. https://doi.org/10.1126/science.aak9997

He Y, Day T, Zhang T, Liu H, Shi X, Chen L, Snyder GJ (2014) High thermoelectric performance in non-toxic earth-abundant copper sulfide. Adv Mater 26:3974–3978. https://doi.org/10.1002/adma.201400515

Jiang Q, Yan H, Khaliq J, Shen Y, Simpson K, Reece MJ (2014) Enhancement of thermoelectric properties by atomic-scale percolation in digenite Cu_xS. J Mater Chem a 2:9486–9489. https://doi.org/10.1039/C4TA01250J

Kanatzidis MG (2010) Nanostructured Thermoelectrics: The New Paradigm? †. Chem Mater 22:648–659. https://doi.org/10.1021/cm902195j

Liang D-D, Ge Z-H, Li H-Z, Zhang B-P, Li F (2017) Enhanced thermoelectric property in superionic conductor Bi-doped Cu1.8S. J Alloys Compd 708:169–174. https://doi.org/10.1016/j.jallcom.2017.02.295

Liu W, Yan X, Chen G, Ren Z (2012) Recent advances in thermoelectric nanocomposites. Nano Energy 1:42–56. https://doi.org/10.1016/j.nanoen.2011.10.001

Lokhande AC, Gurav KV, Jo E, Lokhande CD, Kim JH (2016) Chemical synthesis of Cu 2 SnS 3 (CTS) nanoparticles: a status review. J Alloys Compd 656:295–310. https://doi.org/10.1016/j.jallcom.2015.09.232

Materials Science International Team MSIT®, Ag-Cu-S (silver-copper-sulfur), in: G. Effenberg, S. Ilyenko (Eds.), Non-Ferr. Met. Syst. Part 1, Springer-Verlag, Berlin/Heidelberg, 2006: pp. 1–13. https://doi.org/10.1007/10915981_3

Newman R, Dennis JR, Farrell E (1982) A technical note on Niello. J Am Inst Conserv 21:80–85

Patterson AL (1939) The Scherrer Formula for X-Ray Particle Size Determination. Phys Rev 56:978–982. https://doi.org/10.1103/PhysRev.56.978

Qiu P, Shi X, Chen L (2016) Cu-based thermoelectric materials. Energy Storage Mater 3:85–97. https://doi.org/10.1016/j.ensm.2016.01.009

Sadovnikov SI, Rempel AA, Gusev AI (2018) Nanostructured silver sulfide Ag2S. In: Sadovnikov SI, Rempel AA, Gusev AI (Eds.) Nanostructured lead cadmium silver sulfides. Struct Nonstoichiom Prop. Springer International Publishing, Cham, pp 189–312 https://doi.org/10.1007/978-3-319-56387-9_4

Sharma RC, Chang YA (1986) The Ag−S (Silver-Sulfur) system. Bull Alloy Phase Diagr 7:263–269. https://doi.org/10.1007/BF02869003

Saunders N, Miodownik AP (1998) CALPHAD (calculation of phase diagrams): a comprehensive guide. Pergamon, Oxford

Skinner BJ (1966) The system Cu-Ag-S. Econ Geol 61:1–26. https://doi.org/10.2113/gsecongeo.61.1.1

Skinner BJ, Jambor JL, Ross M (1966) Mckinstryite, a new copper-silver sulfide. Econ Geol 61:1383–1389. https://doi.org/10.2113/gsecongeo.61.8.1383

Tang H, Sun F-H, Dong J-F (2018) Asfandiyar, Zhuang H-L, Pan Y, Li J-F, Graphene network in copper sulfide leading to enhanced thermoelectric properties and thermal stability. Nano Energy 49:267–273. https://doi.org/10.1016/j.nanoen.2018.04.058

Tokuhara Y, Tezuka K, Shan YJ, Imoto H (2009) Syntheses of complex sulfides AgCuS and Ag3CuS2 from the elements under hydrothermal conditions. J Ceram Soc Jpn 117:359–362. https://doi.org/10.2109/jcersj2.117.359

Trots DM, Senyshyn A, Mikhailova DA, Vad T, Fuess H (2008) Phase transitions in jalpaite, Ag_3CuS_2. J Phys

Condens Matter 20:455204. https://doi.org/10.1088/0953-8984/20/45/455204

Wei T-R, Qin Y, Deng T, Song Q, Jiang B, Liu R, Qiu P, Shi X, Chen L (2019) Copper chalcogenide thermoelectric materials. Sci China Mater 62:8–24. https://doi.org/10.1007/s40843-018-9314-5

Zheng X, Liu Y, Du Y, Sun Y, Li J, Zhang R, Li Q, Chen P, Zhao G, Fang Y, Dai N (2018) P-type quaternary chalcogenides of Cu2ZnSn(S, Se)4 nanocrystals: large-scale synthesis, bandgap engineering and their thermoelectric performances. J Alloys Compd 738:484–490. https://doi.org/10.1016/j.jallcom.2017.12.204

Živković D, Ćosović V, Živković Ž, Štrbac N, Sokić M, Talijan N, Boyanov B, Mitovski A (2013) Kinetic investigation of silver sulfide phase transformations. Mater Sci Semicond Process 16:217–220. https://doi.org/10.1016/j.mssp.2012.06.023